Neutron Phase Imaging and Tomography

F. Pfeiffer, C. Grünzweig, O. Bunk, G. Frei, E. Lehmann, and C. David
Paul Scherrer Institut, CH-5232 Villigen PSI, Switzerland
(Received 6 April 2006; published 2 June 2006)

We report how a setup consisting of three gratings yields quantitative two- and three-dimensional images depicting the quantum-mechanical phase shifts of neutron de Broglie wave packets induced by the influence of macroscopic objects. Since our approach requires only a little spatial and chromatic coherence it provides a more than 2 orders of magnitude higher efficiency than existing techniques. This dramatically reduces the required measurement time for computed phase tomography and opens up the way for three-dimensional investigations of previously inaccessible quantum-mechanical phase interactions of neutrons with matter.

DOI: 10.1103/PhysRevLett.96.215505 PACS numbers: 61.12.Ex, 42.25.Fx, 42.30.Rx, 61.43.Gt

For particle physicists, neutrons are small massive particles with a confinement radius of about 10^{-15} m and a distinct internal quark-gluon structure. In quantum mechanics, neutrons are described by de Broglie [1] wave packets whose spatial extent may be large enough to show interference effects similar to what can be observed with visible laser light or highly brilliant x-rays from synchrotron sources. Measurements of the neutron wave packet's phase shift induced by different interaction potentials have a long and distinguished history in the exploration of the fundamental properties of quantum mechanics [2]. If such phase sensitive measurements are further combined with neutron imaging approaches, two- or even three-dimensionally resolved spatial information on the quantum-mechanical interactions of massive particles with matter can be obtained.

Consequently, several attempts have been made to detect the neutron wave optical phase variations induced by an object in the past years. They can be classified into interferometric methods [3–5], techniques using an analyzer crystal [6], and free-space propagation methods [7,8]. However, practical difficulties arise, because the currently available neutron sources are not sufficiently coherent or bright for the effective application of the existing phase sensitive imaging methods. This is because they require monochromatic crystal optics [3–6] or the high spatial coherence of a pinhole source [7,8].

In this Letter we demonstrate how an alternative approach using a grating-based *shearing interferometer* can be efficiently used to retrieve quantitative differential phase contrast (DPC) images with polychromatic neutron sources of little spatial and chromatic coherence. We have recently shown that this method can be used for DPC imaging using polychromatic x rays from synchrotron or tube sources [9,10]. Here we describe, in particular, how taking into account the quantum-optical properties of matter waves allows for a successful adaptation of the latter method to a beam of massive particles, i.e., to neutrons.

Our setup consists of a source grating G0, a phase grating G1, and an analyzer absorption grating G2 [Fig. 1(a)]. The source grating (G0), an absorbing mask with transmitting slits, typically placed close to the neutron beam exit port, creates an array of individually coherent, but mutually incoherent sources. Each individual line source provides enough spatial coherence for the DPC image formation process [11]. Since the source mask G0 can contain a large number of individual lines, each creating a virtual source, efficient use can be made of typical neutron source sizes of more than a few square centimeters. To ensure that each of the line sources contributes con-

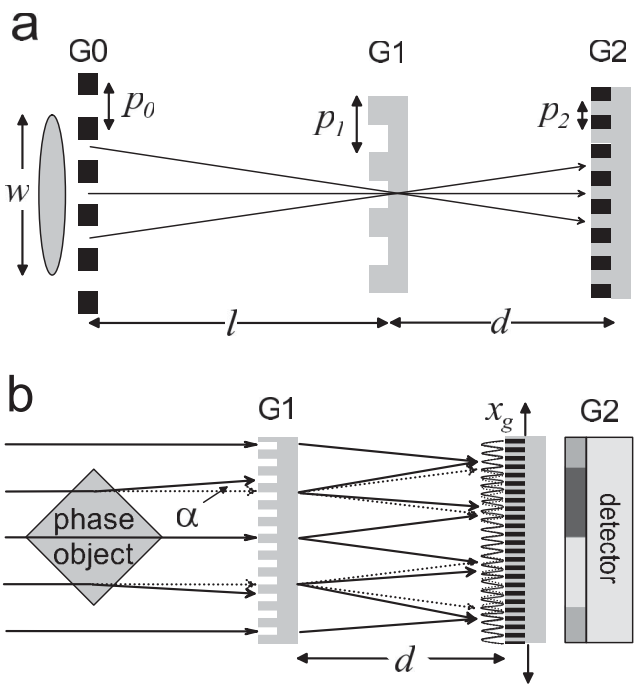

FIG. 1. Grating-based neutron shearing interferometer. (a) The source grating (G0) creates an array of individually coherent, but mutually incoherent sources. (b) The phase grating (G1) forms a periodic interference pattern in the plane of the analyzer grating. A phase object in the incident beam will cause a slight refraction, which results in changes of the locally transmitted intensity through the analyzer.

structively to the image formation process, the geometry of the setup should satisfy the condition: $p_0 = p_2 l/d$, where p_0 (p_2) is the period of G0 (G2), l the distance between G0 and G1, and d the distance between G1 and G2 [Fig. 1(a)]. It is important to note that the total source size w only determines the final imaging resolution, which is given by wd/l. The arrayed source thus decouples spatial resolution from spatial coherence. The DPC image formation process achieved by the two gratings G1 and G2 is similar to *Schlieren* imaging [12] or to a Shack-Hartmann wave-front sensor [13]. The second grating (G1) acts as a beam splitter and divides the incoming beam essentially into the two first diffraction orders. Since the wavelength λ of the illuminating neutron radiation ($\approx 10^{-10}$ m) is much smaller than the grating pitch ($\approx 10^{-6}$ m), the angle between the two diffracted beams is so small that they overlap almost completely.

Downstream of the beam-splitter grating, the diffracted beams interfere and form linear periodic fringe patterns in planes perpendicular to the optical axis [11]. For a phase grating with a phase shift of π, the periodicity p_2 of the fringe pattern equals half the period of G1. Neither the period nor the lateral position of these fringes depends on the wavelength of the radiation used. Perturbations of the incident wave front, such as those induced by refraction on a phase object in the beam, lead to local displacement of the fringes [Fig. 1(b)].

The fundamental idea of the method presented here is to detect the local positions of the fringes and determine from these the phase shift induced by the object. However, since the spacing of the interference fringes does not exceed a few microns, an area detector placed in the detection plane will generally not have sufficient resolution to resolve the fringes, let alone the exact position of their maxima. Therefore, a grating G2 with absorbing lines and the same periodicity and orientation as the fringes is placed in the detection plane, immediately in front of the detector. This analyzer grating acts as a transmission mask for the detector and transforms local fringe position into signal intensity variation. The detected signal profile thus contains quantitative information about the phase gradient of the object. To separate this phase information from other contributions to the signal, such as attenuation in the sample, inhomogeneous illumination or imperfections of the gratings, the phase-stepping approach used in other interferometry methods [2] was adapted to this setup. When one of the gratings is scanned along the transverse direction x_g (see Fig. 1), the intensity signal $I(x, y)$ in each pixel (x, y) in the detector plane oscillates as a function of x_g [Fig. 2(e)]. The interferometer phases $\vartheta(x, y)$ of the intensity oscillations in each pixel are related to the wave-front phase profile $\Phi(x, y)$, the neutron wavelength λ and the period p_2 of the absorption grating by [12]

$$\vartheta = \frac{\lambda d}{p_2} \frac{\partial \Phi}{\partial x}. \quad (1)$$

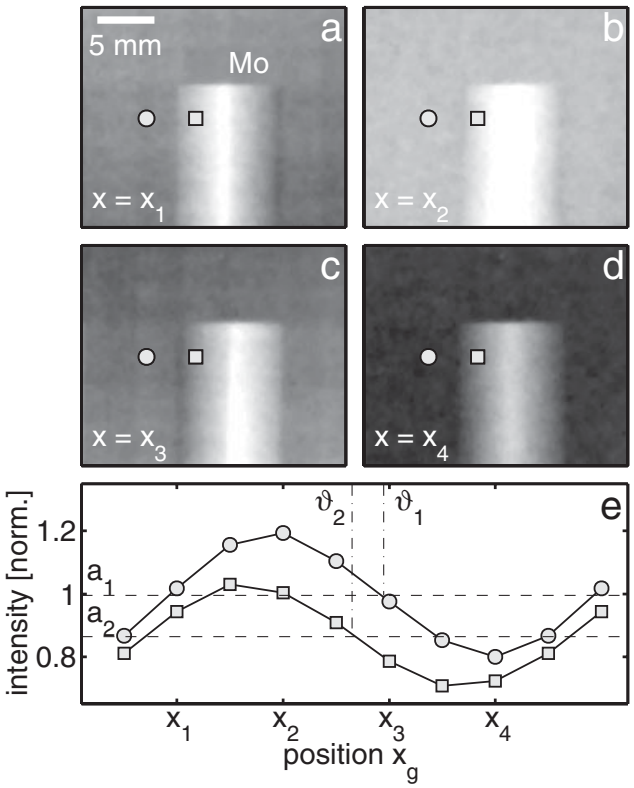

FIG. 2. Principle of phase stepping. (a), (b), (c), (d) Raw image data of a quadratic Mo metal rod, taken at different positions $x_g = x_1, \ldots, x_4$ of the analyzer grating G2. (e) Intensity oscillation in two detector pixels as a function of x_g.

Since ϑ contains no other contributions, particularly no attenuation contrast, the phase profile of the object can be retrieved from $\vartheta(x, y)$ by a simple one-dimensional integration [14]. Another quantity contained in the data from a phase-stepping scan is the average signal for each pixel over an entire oscillation, $a(x, y)$ [Figs. 2(e) and 3(a)]. It is identical to the transmission radiography signal that would be measured without the interferometer. A single phase-stepping scan thus yields both the phase and the attenuation image.

The experiments were carried out at the Swiss Spallation Neutron Source (SINQ) using the beam port of the cold neutron imaging facility (ICON). A 100 mm thick Beryllium filter was used to reject neutrons with wave lengths $\lambda \leq 4.0$ Å, resulting in an incident cold neutron spectrum with a maximum at $\lambda_{\max} \simeq 4.1$ Å and a wave length distribution (FWHM) of $\Delta\lambda/\lambda_{\max} \simeq 25\%$.

The gratings were fabricated using standard photolithography (G0, G1, G2), chemical wet etching (G1, G2) [15], and evaporation of Gadolinium (G0, G2) [16]. They were placed with their lines perpendicular to the optical axis of the setup and parallel to the vertical direction. They had periods of $p_0 = 1.08$ mm, $p_1 = 7.97$ μm, and $p_2 = 4.00$ μm. The distances between the gratings were $l = 5.23$ m and $d = 19.4$ mm. An approximately circular

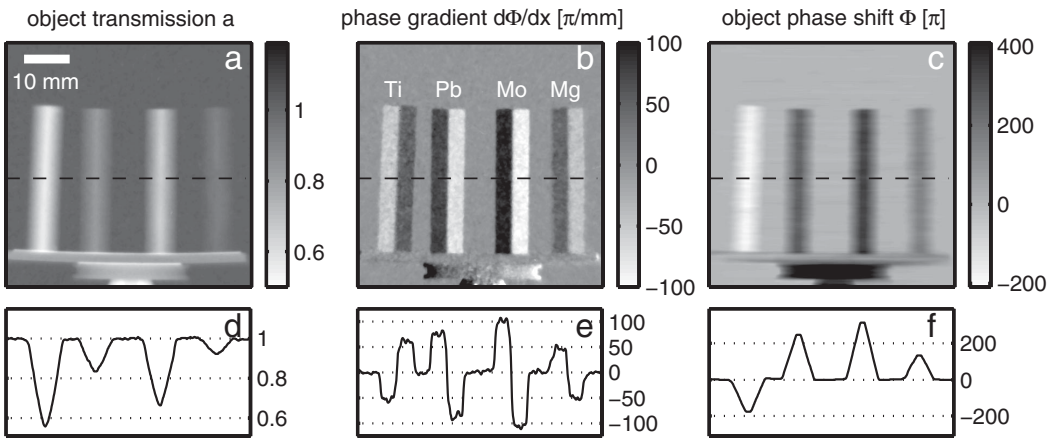

FIG. 3. Linear contour plots and section profiles of processed data for a test object comprising a Ti, Pb, Mo, and Mg metal rod with a quadratic profile. (a) Conventional neutron transmission image. (b) Differential phase contrast image $d\Phi/dx$. (c) Integrated phase shift $\Phi(x, y)$ retrieved from $d\Phi/dx$ by integration. The images are represented on a linear gray scale. (d), (e), (f) Section profiles through the corresponding image data.

source (beam port exit) with a size of $w \simeq 20$ mm was used.

The images were recorded using a 300 μm thick Li-6/ZnS converter and fluorescence screen with a demagnifying optical lens system and a cooled charge coupled device (CCD) [17]. The effective spatial resolution was mainly determined by the intrinsic unsharpness of the scintillation screen to 250 μm. The field of view was 64×64 mm^2 [18]. A typical exposure time for a single raw image was 10 sec; up to ten images were taken per oscillation period in the phase-stepping scan.

Figure 3 shows processed transmission [Fig. 3(a)], DPC [Fig. 3(b)], and integrated phase [Fig. 3(c)] images of a sample comprising a titanium (Ti), lead (Pb), molybdenum (Mo), and magnesium (Mg) metal rod with a quadratic profile [Fig. 1(b)]. Because of their specific neutron capture cross sections and incoherent scattering cross sections, differences in the transmitted intensity through the rods are observed in Fig. 3(a). Since the vector component of the phase gradient in the direction perpendicular to the grating lines is constant, but off opposite signs for both sides of the rods, they appear black and white in the DPC image. It is interesting to note that Ti has a negative neutron scattering length density [19] and consequently a negative phase shift is measured in the material [see Fig. 3(c)]. Furthermore, we note that particularly for weakly absorbing materials, like Mg and Pb [see Fig. 2(a)], the DPC [Fig. 3(b)] and the integrated phase shift [Fig. 3(c)] signal yield a higher contrast in the image.

For a more quantitative comparison, let us consider the exact values for the neutron-nuclear phase shift, which is given by $\Phi = Nb_c\lambda D$, where N is the atom density, b_c is the coherent neutron-nuclear scattering length, and D the thickness of the object in the neutron beam [2]. Using a mean wavelength of $\lambda = 4.1$ Å and literature values for the coherent neutron-nuclear scattering lengths we expect for quadratic rods with an edge length of 5.0 mm values of $d\Phi/dx = \mp 51$ (Ti), ± 81 (Pb), ± 116 (Mo), and ± 61 (Mg) $[\pi/\text{mm}]$. In the case of Ti and Pb, this agrees well with our measurements [Figs. 3(b) and 3(e)]. The slightly smaller measured values for Mo and Mg can be caused by the presence of impurities in the metal samples, decreasing the effective nuclear scattering length density. Particularly the latter aspect sets the basis for further quantitative analysis, such as the reconstruction of a three-dimensional map of the object's nuclear scattering length density by using computerized tomography algorithms. This is particularly important, since the high efficiency [20] of our approach allows for a three-dimensional neutron phase contrast computer tomography within practical time scales of a few hours. As an example, Fig. 4 shows processed DPC [Fig. 4(a)], integrated phase [Fig. 4(b)], and two (out of 512) reconstructed tomographic slices [Figs. 4(c) and 4(d)] through the three-dimensional coherent scattering length density distribution of a sample comprising a Ti and Pb rod of 6.35 mm diameter. One-hundred-eighty phase projections and one reference projection without the sample, each of them containing ten phase-step images (of 10 sec exposure time) were used as an input for a standard filtered backprojection algorithm [21].

In conclusion we have shown how a setup consisting of three transmission gratings can yield quantitative differential phase shift images for beams of massive particles. The presented approach requires only a little spatial and chromatic coherence and thus is significantly [20] more efficient than existing methods. We demonstrate the capabilities by presenting, for the first time, a full three-dimensional reconstruction of the scattering length density distribution of a test sample obtained within a few hours. Based on these results we conclude that our method represents a major step forward in phase radiography and computed phase tomography with matter waves. It particu-

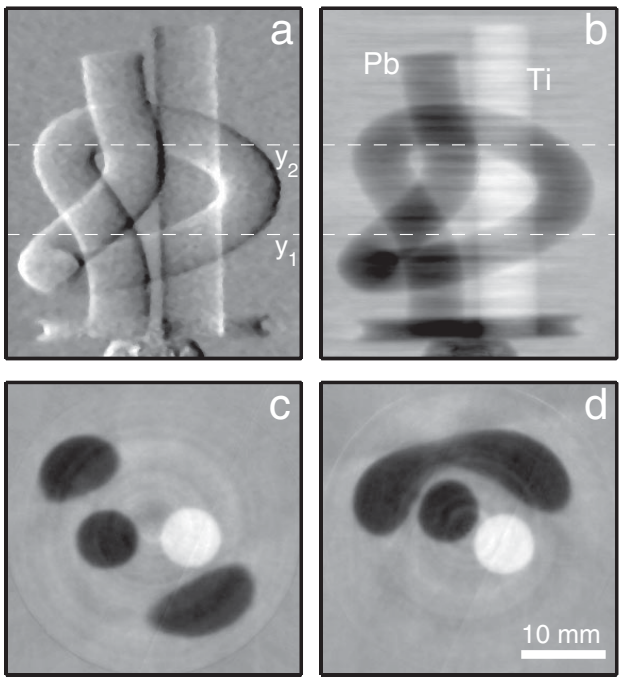

FIG. 4. Projection images and tomographic slices for a sample comprising a Pb and Ti rod with a diameter of 6.35 mm. (a) Differential phase contrast, and (b) phase shift projection image. (c), (d) Two (out of 512) reconstructed tomographic slices through the three-dimensional coherent scattering length distribution in the sample. The total exposure time was 240 min.

larly opens up the way for imaging the neutron quantum-mechanical phase shifts induced by more than just the nuclear interaction. For example, two- or even three-dimensional imaging of the magnetic domain structures inside macroscopic objects based on the interaction of the neutron spin with the magnetic field [22–24] or spatially resolved dynamic studies based on the neutron Fizeau effect [25] can be envisioned. Finally, this work could provide the basis for bridging the gap between imaging and quantum-optical investigations with other matter waves, such as protons, atoms, or molecules [26].

We gratefully acknowledge the assistance of J. Bruder, X. Donath, and I. Johnson in the measurements and T. Weitkamp, H. Rønnow, and K. Clausen for fruitful discussions.

[1] A. F. Kracklauer, Ann. Phys. (Paris) **10**, III (1925).
[2] H. Rauch and S. A. Werner *Neutron Interferometry* (Oxford University Press, Oxford, 2000).
[3] M. Zawisky, U. Bonse, F. Dubus, Z. Hradil, and J. Rehacek, Europhys. Lett. **68**, 337 (2004).
[4] F. Dubus, U. Bonse, M. Zawisky, M. Baron, and R. Loidl, IEEE Trans. Nucl. Sci. **52**, 364 (2005).
[5] J. Rehacek, Z. Hradil, M. Zawisky, U. Bonse, and F. Dubus, Phys. Rev. A **71**, 023608 (2005).
[6] W. Treimer, M. Strobl, A. Hilger, C. Seifert, and U. Feye-Treimer, Appl. Phys. Lett. **83**, 398 (2003).
[7] B. E. Allman, P. J. McMahon, K. A. Nugent, D. Paganin, D. L. Jacobson, and S. A. Werner, Nature (London) **408**, 158 (2000).
[8] P. J. McMahon, B. E. Allman, M. Arif, S. A. Werner, and K. A. Nugent, Phys. Rev. Lett. **91**, 145502 (2003).
[9] T. Weitkamp, F. Pfeiffer, P. Cloetens, M. Stampanoni, and C. David, Opt. Express **13**, 6296 (2005).
[10] F. Pfeiffer, T. Weitkamp, O. Bunk, and C. David, Nature Phys. **2**, 258 (2006).
[11] F. Pfeiffer, O. Bunk, T. Weitkamp, J. F. van der Veen, and I. K. Robinson, Phys. Rev. Lett. **94**, 164801 (2005).
[12] M. Born and E. Wolf, *Principles of Optics* (Pergamon Press, Oxford, 1980).
[13] J. Hartmann, Z. Instrumentenkd **8**, 2 (1990).
[14] In the general case in which the incident wave front already shows some distortion, the background phase should be measured (with the object removed from the beam) and then subtracted. Provided that the sample is smaller than the field of view, the integration constants are known and the phase function is uniquely defined.
[15] C. David, E. Ziegler, and B. Nöhammer, J. Synchrotron Radiat. **8**, 1054 (2001).
[16] C. Grünzweig *et al.* (to be published).
[17] Fingerlakes Instruments (FLI IMG 1001, KODAK chip with 1024×1024 pixels, 24×24 μm^2 pixel size).
[18] The field of view was determined by the 100 mm wafer processing technology, with which the gratings were fabricated in our case. No principle constraints hinder the upscaling by using state-of-the-art (300 mm) techniques.
[19] V. F. Sears, Neutron News **3**, 26 (1992).
[20] An exposure time of 12 h for a single phase projection measured at an equivalent neutron source (National Institute of Standards) is reported in Ref. [8]. In Ref. [4], a value of 2 h per image at a 5–10 times more intense neutron source (Institute Laue-Langevin) is stated. We conclude that our method, which requires typically 10 images of 10 sec exposure time for a single projection, yields a decrease in exposure times by more than a factor of hundred.
[21] A. C. Kak and M. Slaney, *Principles of Computerized Tomography* (IEEE Press, New York, 1987).
[22] M. Schlenker, W. Bauspiessl, W. Graff, U. Bonse, and H. Rauch, J. Magn. Magn. Mater. **15–18**, 1507 (1980).
[23] H. Hochhold, H. Leeb, and G. Badurek, J. Magn. Magn. Mater. **157**, 575 (1996).
[24] G. Badurek, R. J. Buchelt, and H. Leb, Physica (Amsterdam) **276–278B**, 588 (2000).
[25] A. G. Klein, A. Cimmino, A. Zeilinger, W. Treimer, and R. Gähler, Phys. Rev. Lett. **46**, 1551 (1981).
[26] M. Arndt, O. Nairz, J. Vos-Andreae, C. Keller, G. van der Zouw, and A. Zeilinger, Nature (London) **401**, 680 (1999).